Research Square

Preprints are preliminary reports that have not undergone peer review.
They should not be considered conclusive, used to inform clinical practice,
or referenced by the media as validated information.

Cell senescence emerges as a hallmark and therapeutic target of chronic intracellular infection

Edoardo Scarpa

edoardo.scarpa@unimi.it

University of Milan

Doriana Oliveri

University of Milan https://orcid.org/0009-0006-3300-6638

Diego Rondelli

University of Milan https://orcid.org/0000-0002-7178-6843

Carla Chernichero

IRCCS San Raffaele Scientific Institute

Federico Russo

University of Milan

Riccardo Nodari

University of Milan https://orcid.org/0000-0002-3485-2485

Giorgia Moschetti

University of Milan

Anna Griego

University of Milan https://orcid.org/0000-0003-4887-6645

Marta Zaccaria

University of Milan https://orcid.org/0000-0002-7171-6706

Federico Di Marco

IRCCS San Raffaele Scientific Institute

Fabio Saliu

IRCCS San Raffaele Scientific Institute

Gabriele Marchello

Istituto italiano di Tecnologia

Ferdinando Cannella

Istituto italiano di Tecnologia

Manuel Albanese

University of Milan

Gianluca Cidonio

University of Rome La Sapienza https://orcid.org/0000-0002-9445-6994

Lara Manganaro

University of Milan
Daniela Cirillo
IRCCS San Raffaele Scientific Institute https://orcid.org/0000-0001-6415-1535
Raffaele De Francesco
University of Milan https://orcid.org/0000-0001-8754-5123
Sergio Abrignani
University of Milan
Raffaella Di Micco
IRCCS San Raffaele Scientific Institute https://orcid.org/0000-0002-0639-8238
Nicola Lorè
IRCCS San Raffaele Scientific Institute https://orcid.org/0000-0001-9159-1632
Loris Rizzello
University of Milan

Article

Keywords:

Posted Date: January 21st, 2026

DOI: https://doi.org/10.21203/rs.3.rs-8377374/v1

License: This work is licensed under a Creative Commons Attribution 4.0 International License.
Read Full License

Additional Declarations: There is **NO** Competing Interest.

Abstract

Intracellular pathogens are ideal candidates for modelling the pathophysiology of chronic infection, as they hide within host cells and avoid conventional immune clearance through a controlled reshaping of cellular fate. This study unveils how the emerging intracellular pathogen Mycobacterium abscessus (Mab) reprograms alveolar macrophages towards a senescent state -a complex multifaced phenotype marked by proliferative arrest, distinctive morphological shifts, activation of DNA damage signalling cascade, and secretion of senescence-associated secretory phenotype (SASP) factors. Mab-induced DNA damage emerged as the primary driver of senescence, while SASP secretion acts as a molecular broadcaster, propagating secondary senescence in neighbouring, uninfected cells through paracrine signalling. This cascading wave of amplified senescence underscores a detrimental effect on the tissue microenvironment, potentially turning it into a chronic inflammatory niche that facilitates Mab persistence and immune evasion. By leveraging on the evidence of chronic infection-induced senescence, we prototyped a therapeutic approach where senolytic drugs selectively eradicated senescent cells and significantly reduced bacterial burden, similarly to antibiotics. This work molecularly dissects a previously overlooked axis of chronic infection-triggered senescence, wherein pathogen-induced DNA damage serves as the initiating event for starting the senescence program in host immune cells. More importantly, the results presented here demonstrate that eliminating infected senescent cells constitutes an unprecedented and effective host-directed therapy that can enhance treatment outcomes while bypassing the limitations imposed by rising antimicrobial resistance.

Introduction

Intracellular pathogens represent one of the most significant selective pressures in the evolutionary trajectory of humans, and of other multicellular organisms, as they shape and drive the co-evolutionary dynamics between hosts and pathogens[1,2].

Bacteria establish intimate interactions with (and within) their hosts, often giving rise to evolutionary arms races[2,3]. While hosts have evolved mechanisms to detect, contain, and eliminate intracellular bacteria[4], the latter developed strategies to evade immune surveillance, and subvert eukaryotic cellular pathways to establish a replicative niche[5]. During early colonisation, pathogens secrete a repertoire of virulent determinants that modulate host cellular signalling pathways to enhance microbial survival, persistence, and replication[6,7]. These virulence factors are meant to facilitate immune evasion while also contributing to host tissue damage and dysfunction[8,9]. In addition to such direct actions, pathogenic determinants can indirectly induce damage through a dysregulated, or excessive, immune activation that can result in host-mediated pathology, leading to persistent tissue injury even long after microbial clearance[10]. Despite the clinical relevance of infection resolution, the long-term cellular and immunological consequences of chronic infections remain significantly uncharacterised. A mechanistic understanding of how pathogens establish long-term residence within host tissues is critical for elucidating the intercellular interactions between immune and tissue-resident cell populations.

We argued that such a long-lasting and complex interplay should raise significant questions about the final fate of chronically infected immune cells, and hypothesised that cellular senescence could represent one potential, yet significantly underexplored, outcome[11].

Senescent cells, while no longer dividing due to a stable cell cycle arrest, remain metabolically active and exhibit marked resistance to apoptosis[12]. A hallmark feature of these cells is the development of the senescence-associated secretory phenotype (SASP), characterised by the sustained secretion of pro-inflammatory cytokines and chemokines (typically, IL-1α, IL-1β, and IL-6, TNF-)[13].

Triggered by DNA damage, telomere attrition, and aberrant oncogene activation, senescent cells have been described in various pathological conditions, such as ageing, cancer, and inflammation[14]. Nevertheless, these cells are also recently emerging as one potential key player during infectious diseases[15,16].

This connection became clear a few years in the context of viral infection, as many virus hijack host machineries, cause DNA damage, or interfere with the DNA damage response (DDR), all of which are typical triggers of senescence[17–19].

Toxins derived from bacteria were also shown to promote senescence via mitochondrial genotoxicity[20], whereas cell senescence induced by a sustained bacterial infection was observed only very recently[21,22]. Nevertheless, the molecular mechanism linking the persistent insult from a pathogen to the onset of senescence remains unclear, a question we aimed to address here.

We adopted *Mycobacterium abscessus* (*Mab*) as our model microbial system, given its rapid growth, rising prevalence in clinical settings, and well-documented innate resistance to antimicrobials [23,24]. *Mab*, as many other Mycobacteria, hides and proliferates inside macrophages making it a perfect candidate to test our hypothesis that chronic infection causes senescence.

We initially developed an *in vitro* system mimicking chronic *Mab* infection in murine alveolar-like macrophages. Over time, we observed that the host cells respond with a slow but definitive shift into senescence. Although functionally arrested, these cells secrete a potent SASP cocktail, rich in inflammatory mediators, that drives paracrine senescence in neighbouring, uninfected cells. We identified *Mab*-induced DNA damage as the key molecular trigger initiating this senescence program. Spatial transcriptomics of lung tissue from a mouse model of *Mab* chronic infection revealed a sustained expression of senescent gene signatures within infected regions enriched in macrophages. These findings validated the relevance of our *in vitro* findings and established a clear link between chronic infection and the emergence of senescence *in vivo*. Building on this, we showed that senolytic therapy restores pro-apoptotic signalling in senescent cells and effectively reduces bacterial burden by targeting the removal of senescent macrophages.

Notably, senolytic therapy outperformed antibiotics under certain *in vitro* conditions and retained efficacy *in vivo*. Together, our results uncover a previously unrecognised mechanism by which chronic bacterial infection induces host cell senescence via DNA damage. This also positions infection-induced senescence as a central feature of host–pathogen interactions and identifies senolytics as a promising host-directed therapeutic strategy against chronic bacterial infections in the context of rising antimicrobial resistance.

RESULTS

Model of chronic *Mab* infection *in vitro*. To test whether chronic intracellular infection by *Mab* drives macrophage senescence, we established an *in vitro* model using murine macrophages (MPI cells). These self-renewing cells recapitulate key features of tissue-resident AM, the primary niche for *Mab* infection, and offer a tractable system to interrogate host–pathogen interactions[25,26]

To capture both early and sustained host responses, we optimised a protocol enabling prolonged infection and culture for up to 5 days post-infection. This was achieved by exposing MPI cells to a low multiplicity of infection (MOI 1:0.25) of a fluorescent *Mab* strain constitutively expressing tdTomato. To prevent extracellular bacterial overgrowth and cytotoxicity, we limited the exposure to the pathogen to 2 hours, followed by extensive washing. After 3 days, cultures were maintained with daily washes and fresh media to remove residual extracellular bacteria (Fig. 1a). This setup permitted assessment of host responses at day 1 (representing acute exposure) and day 5 (which hereafter refer to as chronic infection to reflect prolonged intracellular bacterial persistence within macrophages) , while maintaining a physiologically relevant, intracellularly focused infection model. Henceforth, we refer to "*Mab* exposed" as the experimental group comprising cells insulted with the pathogens, and to "Mab^{+}" as the specific subgroup of cells that host the bacteria, to distinguish them from those insulted but not carrying *Mab* ("Mab^{-}").

With this model, we yielded a stably progressive infection of MPI, with 22 ± 6% of Mab^{+} cells at day 1, and 65 ± 13% at day 5 (Fig. 1b,c). Alongside, we observed an increase in intracellular bacterial load over time (Fig. 1d).

We first aimed to evaluate phenotypic changes in host cells following chronic infection by high-content image-based morphological profiling. A total of 32 features (*e.g.* cell area, perimeter and mean radius) were quantified, and Z-scores were computed relative to the pooled distribution across conditions (Uninfected *Vs Mab* exposed) and the two time points[27] (Extended Table 1). *Mab* exposed cells exhibited a distinct morphological profile at day 5 relative to uninfected controls, as shown by median feature clustering (Fig. 1e). Dimensionality reduction revealed two segregated populations with divergent morphologies (Fig. 1f), including pronounced shifts in cell area and circularity (Fig. 1g,h). Notably, chronically *Mab* exposed MPI also changed nuclear morphology compared to uninfected controls, with Mab^{+} cells showing increased nuclear irregularity and size variation (Extended Data Fig. 1a-f), which indicates widespread remodelling of nuclear architecture in response to prolonged infection.

These findings suggest that prolonged exposure to the pathogen induces morphological alterations, potentially reflecting more profound biological reprogramming. We next examined whether long-term *Mab* exposure impacted host-cell proliferation. Under standard conditions, MPI cells retain replicative capacity, consistent with their reported phenotypic similarity to resident alveolar macrophages (Extended Data Fig. 1i-k)[25,26]. However, EdU incorporation and Ki67 expression assays revealed a marked decline in proliferation following *Mab* infection, with only ~2% of cells progressing through S-phase, and a significant reduction in the $Ki67^+$ population by day 5 (Fig. 1 i-n). This reduced proliferation was observed in both Mab^+ and Mab^- cells within the same experimental group (Fig. 1k,n). Notably, increasing the MOI (from 1:0.25 to 1:0.5) elevated the infection burden and similarly suppressed proliferation, but significantly compromised cell viability at later time points, thus it was not further evaluated (Extended Data Fig. 1g,h). Together, these morphological and proliferative changes raised the possibility that chronic infection may induce a senescence-like state in macrophages.

Chronic *Mab* infection induces cellular senescence in macrophages. To investigate whether long-term infection induces a senescence program, we performed bulk RNA-seq on MPI exposed to *Mab* in acute and chronic conditions, alongside time-matched uninfected controls. Chronic exposure to the pathogen caused widespread changes in gene expression reprogramming compared to both acute infection and uninfected controls (Fig. 2a; see Extended Data Fig. 2a for all contrasts). We then asked whether such transcriptional landscape reflected typical senescence programs. Indeed, chronic Mab exposure induced a coordinated reprogramming of the SenMayo gene panel [28], involving both upregulated and downregulated transcripts associated with cellular senescence. In contrast, acute infection and uninfected controls remained largely unchanged (Fig. 2b).

We validated the RNA-seq findings, demonstrating that chronic conditions upregulate Cdkn1a and Trp53, and downregulate Lmnb1, all key senescence markers[29,30](Fig. 2c; Extended Data Fig. 2b). Consistently, gene set enrichment analysis (GSEA) revealed strong enrichment of the SenMayo signature in chronically exposed cells (Fig. 2d). This result was also validated across multiple published senescence-related panels, further confirming the enriched senescence signature in chronic conditions (Extended Table 2 and Extended Data Fig 2c, d). Ingenuity Pathway Analysis (IPA) of chronically exposed cells revealed significant activation of senescence pathway signalling, alongside ECM remodelling, pro-inflammatory pathways (Cytokine Storm, IL-6), Interferon signalling, and G2/M DNA damage checkpoint. Conversely, proliferative pathways and DNA repair mechanisms (TP53 Activity Regulation, NER, BER) were suppressed (Fig. 2e). Complementary pathway enrichment analysis confirmed upregulation of Interferon & Antiviral Response, Inflammatory Signalling, Immune Cell Activation, and ECM remodelling (characteristic of SASP), while cell cycle and DNA Damage & Repair pathways were markedly downregulated (Fig. 2f).

To confirm that these transcriptional changes translate into a functional senescent phenotype, we next examined protein-level markers of senescence. Expression of the cyclin-dependent kinase inhibitor p21 was significantly increased in Mab-exposed macrophages at day 5, whereas uninfected controls maintained stable expression throughout the experiment ($p < 0.0001$; Fig. 2g,h). Among Mab^+, the

proportion of p21⁺ cells significantly increased at day 5 ($p < 0.0001$; Fig. 2i), in agreement with gene expression data. Furthermore, we assessed senescence-associated β-galactosidase (SA-β-gal) activity, a widely used marker of cellular senescence[29,31]. To reduce baseline β-galactosidase activity in macrophages[32], we employed a pre-treatment protocol using bafilomycin to inhibit endogenous lysosomal activity (Extended figure 2e). *Mab*-exposed cells exhibited robust cytoplasmic SA-β-gal staining (Fig. 2j), with the proportion of positive cells rising steadily over time ($p < 0.0001$; Fig. 2k). Most of Mab^+ cells (~75%) were also SA-β-gal⁺ (Fig. 2l), suggesting that senescence primarily affects bacteria-harbouring macrophages. Nonetheless, a considerable fraction of SA-β-gal⁺ cells lacked detectable intracellular bacteria, suggesting potential paracrine diffusion of senescence.

These findings demonstrate that chronic intracellular infection with Mab drives macrophages into a *bona fide* senescent state, characterised by coordinated transcriptional reprogramming, cell cycle arrest, lysosomal activation, and nuclear remodelling.

DNA-damage response to chronic *Mab* exposure. Since the presence and accumulation of DNA damage is one inducer of cellular senescence, we investigated the activation of DDR markers. Immunofluorescence staining of both γH2A.X and 53BP1 (Fig. 3a) revealed that chronic exposure to *Mab* induced an increase in the average number of nuclear foci, compared to the uninfected control (Fig. 3b,c). No significant differences in γH2A.X foci were observed between Mab^+ and Mab^- subpopulations (Fig. 3d), while the number of 53BP1 foci was slightly higher in Mab^+, suggesting that the activation of DDR is not exclusive to cells hosting the pathogen (Fig. 3e).

Although we did not observe a robust DDR activation in MPI cells under acute conditions, we confirmed the presence of DNA damage in other cell types following 24 hours exposure to *Mab*. This suggests that the lack of a strong early response might be specific to MPI cells (Extended Data Fig. 3 a-h).

To distinguish whether the activation of γH2A.X was triggered by single or double-strand DNA breaks, we assessed autophosphorylation levels of ATM/DNA-PK (double-strand breaks) and ATR (single-strand breaks). While we did not observe differences in phosphorylation of these kinases in *Mab* exposed cells during acute conditions, the analysis *of the* Mab^+ subgroup revealed a mild activation (Extended data Fig.3i-n). Conversely, under chronic conditions all kinases were activated (Fig. 3f-h), with DNA-PK playing the predominant role in Mab^+ subpopulation (Fig. 3i-k). We next performed the comet assay to confirm the presence of DNA damage, and to discriminate between exclusively single-strand, or a mix of single- and double-strand DNA breaks. Chronically exposed cells displayed a significant increase in tail moment under alkaline conditions, indicative of both single- and double-strand DNA breaks. In neutral comet assays, where only double-strand breaks can be detected, we also observed significant migration, suggesting the presence of heterogeneous damage (Fig. 3l, Extended data Fig.3 o,p). Since no differences in tail moment were measured in acute conditions, DNA damage is likely to either accumulate over time or be induced only if the infection reaches a chronic stage (Extended data Fig.3 o,p). Finally, we questioned whether DNA damage is the result of an active process triggered by the intracellular mycobacterium, or a host response to its presence. To assess this, we infected MPI with

propiolactone-fixed *Mab*. The rise in γH2A.X foci occurred only when live *Mab* was present, indicating that live mycobacteria are essential to trigger the DDR (Fig. 3m).

The data collected suggests that *Mab* actively causes the accumulation of DNA damage and triggers DDR, which is likely responsible for the onset of cellular senescence in the host.

Paracrine transmission of senescence from infected cells. Having established that chronic *Mab* infection induces cellular senescence in macrophages, we next explored the functional consequences of this state. A key hallmark of senescent cells is the SASP, characterised by the sustained release of pro-inflammatory cytokines, chemokines, growth factors, and proteases[34]. Beyond altering the local tissue environment, the SASP can drive secondary senescence in neighbouring cells through paracrine signalling[34–36]. We therefore investigated whether senescent macrophages, chronically exposed to *Mab*, secrete SASP, and whether these factors induce senescence in surrounding uninfected cells.

MPI chronically exposed to *Mab* upregulated a panel of canonical SASP genes, including pro-inflammatory cytokines (*e.g.,* Tnf, Il6, Il1-alpha and Il1-beta), chemokines (Cxcl2, Cxcl3, CCL7), matrix remodelling enzymes (Mmp2, Mmp3) and extracellular matrix components (*e.g.,* collagens) (Extended Data Fig. 4a).

To characterise the temporal evolution of the SASP program triggered by *Mab*, we performed comprehensive GSEA comparing acute (day 1) and chronic (day 5) infection. This analysis revealed both unique biological signatures specific to each infection stage, and core pathways that were persistently enriched across both time points (Extended Data Fig. 4b). Network visualisation of the transcriptional programs showed that acute infection is characterised by an activation of transient immune responses (complement activation, dendritic cell activation, regulation of secretion, and antiviral defense). In both acute and chronic phases, we observed a stable inflammatory signature, representing the core inflammatory SASP (NF-κB and pattern recognition receptor (PRR) signalling, altered autophagy, antimicrobial activity, and interferon/antiviral responses).

Chronic infection uniquely induced a suite of late-developing SASP features that were absent during acute infection. These encompassed ECM remodelling (fibrinolysis, coagulation, protease/antiprotease balance, tissue degradation), metabolic reprogramming (lipid accumulation, MAPK signalling, VEGF signalling, TGF-β/BMP inhibition), and sustained type I interferon regulation (Fig. 4a). This temporal progression demonstrates a fundamental shift from acute antimicrobial defence to a complex, tissue-remodelling senescent phenotype, characteristic of chronic infection. Upstream analysis of transcription factor (TF) activity in chronically infected cells revealed the regulatory architecture underlying this SASP program. Chronic *Mab* exposure activated master inflammatory regulators including interferon regulatory factors (IRF3, IRF7, IRF9), NF-κB family members (RELA, NFKB1, NFKBIZ), and STAT1, which

coordinated expression of SASP-related gene programs (Fig. 4b). Additional upregulated regulators included TEA domain transcription factors, the hypoxia-inducible factor (HIF1A), and immune regulators (SPI1, CTNNB1). This indicates convergent activation of inflammatory, hypoxic, and stress response pathways, all of which are molecular signatures that distinguish senescence-associated inflammation from classical acute immune responses (Fig. 4b, Extended Data Fig. 4c).

We next aimed to determine whether the SASP profile observed during chronic infection could be equally mimicked by a classic macrophage activation, induced by sustained extracellular lipopolysaccharide (LPS) stimulation. Macrophages exposed to high-dose of LPS (1 µg/mL) exhibited an acute transcriptional response that significantly diminished in chronic conditions (Extended Data Fig. 4d). In contrast, *Mab* triggered a delayed but progressively intensifying pro-inflammatory signature, characteristic of a senescence-associated response, and clearly distinct from a classical, LPS-like, activation (Extended Data Fig. 4d). These transcriptional trends were also corroborated at the protein level. ELISA measurements revealed robust and sustained secretion of TNFα and IL-6 in chronically *Mab* exposed cells, exceeding the levels observed under a range of LPS doses and stimulation time (Fig. 4c). These observations suggest that, rather than inducing a typical fast-resolving inflammatory response, chronic *Mab* infection elicits a sustained SASP-like response arising from the senescent state of the host cells.

Senescence can propagate to neighbouring cells via paracrine signalling, a process called secondary senescence[35,37]. We then questioned whether senescence could spread from infected to bystander uninfected cells, and analysed the spatial relationship between them. Specifically, the percentage of *Mab*$^-$ but SA-β-gal$^+$ cells was calculated within a radius of 60 or 120 µm of *Mab*$^+$ cells, corresponding to a 2- or 4-cell distance (Fig. 4d). A large proportion of uninfected cells adjacent to *Mab*$^+$ cells were SA-β-gal$^+$ (85.7% ± 14.3%), indicating that senescence tends to cluster around infection sites (Fig. 4e). Uninfected macrophages were treated with conditioned media (CM) collected from cultures chronically exposed to *Mab*, to confirm whether secreted factors are sufficient to trigger senescence. After filtration to remove residual extracellular bacteria, CM was added at increasing concentrations. Microscopy analysis revealed a progressive increase in cytoplasmic SA-β-gal staining in recipient cells, consistent with a senescence phenotype (Fig. 4f). Quantification confirmed a dose-dependent response, with up to ~75% of cells becoming SA-β-gal$^+$ within 48 hours when exposed to 75% (v/v) CM, an effect maintained at 72 hours (Fig. 4g-h). Media from filtered *Mab* cultures, used as control, failed to induce comparable levels of SA-β-gal$^+$ cells over time, similar to CM from MPI cultured for 5 days or fresh culturing media (Fig. 4g).

These findings demonstrate that soluble mediators secreted during chronic infection — and not factors released by extracellular *Mab* or baseline macrophage secretions — are responsible for the paracrine induction of senescence in surrounding cells. Moreover, exposure to CM derived from chronically *Mab*-exposed cells also increased susceptibility to infection. Macrophages exposed to CM for 72 hours

showed a significantly higher level of *Mab* infection after challenge compared to cells cultured in fresh media, CM from uninfected macrophages, or CM from *Mab* cultures (Fig. 4i, Extended Data 4e).

This suggests that paracrine signalling from infected, senescent cells may prime neighbouring cells to become more permissive to infection, potentially amplifying the spread and impact of *Mab* within the tissue microenvironment.

Senolytic treatment reduces bacterial burden. Given that chronically infected senescent cells may serve as a persistent bacterial reservoir, we investigated whether selectively eliminating these cells could promote bacterial clearance in our chronic *Mab* infection model. We designed a sequential treatment protocol combining standard antibiotic therapy with senolytic agents (Fig. 5a). Following 4 days of infection, we first applied standard antibiotic therapy (Amikacin, Amk) to clear extracellular bacteria, then administered the senolytic agent navitoclax (Nav; a Bcl-2 family inhibitor) to selectively eliminate the remaining infected senescent cells (Extended Fig. 5a).

Nav treatment induced a time-dependent increase in caspase-3$^+$ cells, beginning at ~6 hours and reaching maximal levels by 24 hours, compared to untreated or Amk-only controls (Fig. 5b,c and Extended Fig. 5b). This was accompanied by a corresponding decrease in total cell number over the treatment period, consistent with selective cell clearance (Fig. 5d). Nav induced a significant reduction in the percentage of SA-β-gal$^+$ and p21$^+$ cells compared to untreated cultures (Fig. 5e,g), with the greatest effect observed on *Mab*$^+$ populations, confirming senolytic activity (Fig. 5f,h). Importantly, Nav also reduced *Mab*$^-$ populations, likely due to the clearance of secondary bystander senescent cells generated through paracrine SASP spreading.

Having confirmed that Nav eliminates both infected and bystander senescent cells, we next assessed whether this senolytic intervention impacts bacterial burden. Nav treatment significantly lowered the percentage of *Mab*$^+$ cells by apoptosis (Fig. 5i, Extended Data Fig. 5c), and reduced the intracellular bacterial burden, as assessed by quantifying *Mab*-fluorescence intensity *per* cell area (Fig. 5j). Quantification of viable bacteria by colony-forming units (CFUs) assay confirmed a significant reduction in intracellular bacterial load following Nav treatment (approximately 2.3 $\log_{10}$ CFUs reduction, corresponding to ~190-fold decrease). This effect was not observed with Amk alone, and was comparable in magnitude to that achieved with clarithromycin, the current standard of care for treating *Mab* infections (Fig. 5k, Extended Fig.5e). As expected, nav treatment did not directly reduce extracellular bacterial counts, as it targets the infected host cells rather than the pathogen (Extended Fig.5f). In contrast, Amk directly eliminates extracellular bacteria (Fig. 5l). Importantly, the senolytic did not increase extracellular bacterial levels compared to untreated controls, indicating that apoptotic elimination of infected senescent cells does not release viable intracellular bacteria into the surrounding environment (Fig. 5l). Together, these findings show that senolytic targeting of infected senescent macrophages reduces the intracellular bacterial burden without spreading infection.

Senescent processes in mouse model of *Mab* chronic infection. Having demonstrated the onset of cellular senescence in our *in vitro* model, we next asked whether similar mechanisms also occur *in vivo* during chronic respiratory *Mab* infection. We used an established mouse model, based on agar beads (Fig. 6a), that replicates bacterial persistence in granuloma-like structures, a classic hallmark of mycobacterial infections, and elicits a wide range of inflammatory responses in the airways and parenchyma[38,39] (Fig. 6b). We assessed the expression of the SenMayo transcriptional signature in chronically infected lung tissues by spatial transcriptomics analysis of a previously published dataset profiling dual host-pathogen gene expression (GEO accession number GSE242471). We quantified the senescence signature score across tissue regions and evaluated the expression of individual signature genes within each defined tissue cluster (Fig. 6c).

Indeed, unsupervised cluster analysis of gene expression identified 4 clusters shared between control and infected mice (S1, S2, S3, and S4) and 3 clusters exclusive to chronically infected mice (I1, I2, and I3) (Extended Data Figure 6a,b).

SenMayo signature was predominantly enriched within host-driven pathological clusters (I1), which are characterised by chronic inflammation (Fig. 6d). A subset of this gene set, including the canonical senescence marker Cdkn1a, was markedly upregulated in inflammatory clusters (Fig. 6e), and remained significantly elevated within granuloma-like structures (Fig. 6f). The interrogation of this dataset enabled simultaneous spatial analysis of both host and pathogen transcriptional programs. Senescence signature expression was significantly higher in *Mab*$^{+}$ regions (spots containing bacterial transcripts), suggesting that bacterial persistence contributes to the activation of senescence pathways (Fig. 6g). To validate these transcriptomic results at the protein level, we examined p21 expression in a new cohort of mice chronically infected with *Mab* (Extended Data Figure 6c). After 21 days, p21 levels were significantly elevated in infected lungs, especially in areas with pathological tissue (Fig. 6h). The count of p21^{+} cells per mm² showed a notable increase in inflamed and infected regions compared with non-inflamed parenchyma, supporting the presence of localised senescence activation *in vivo* (Fig. 6i). Taken together, these results demonstrate that a senescence transcriptional program is activated during chronic *Mab* infection, and that p21 may represent a reliable marker of pathological regions where these processes are engaged by persistent bacterial infection.

Finally, we tested whether senolytic treatment would reduce bacterial burden in this chronic model. Mice were daily administered with Nav starting from day 7 post-infection, which is the time needed to establish a chronic infection. Despite the considerable inter-individual variability, Nav treatment significantly reduced pulmonary bacterial burden compared with untreated controls, though the magnitude of this effect was more modest than with Amikacin treatment (Fig. 6jConcurrent administration of nav with Amikacin did not improve outcomes (Extended Data Fig. 6d), suggesting that rapid antibiotic-mediated killing of extracellular bacteria could limit the senolytic contribution.

These results provide proof of concept for senolytic therapy as an adjunctive strategy to complement antibiotic treatment, targeting the senescent cell niche that sustains chronic infection rather than the

pathogen itself.

Discussion

Chronic infections pose significant challenges in infectious disease biology, particularly when prolonged host-pathogen interactions lead to tissue remodelling, immune escape, and persistent pathogen survival. Here, we report a previously unrecognised host response to chronic *Mab* infection, namely the induction of cellular senescence in alveolar macrophages. While senescence has been studied extensively in the context of cancer and aging, and only recently in viral infections, its role in chronic bacterial infections has remained largely unexplored. Our findings expand this paradigm of pathogen-induced senescence and illuminate new molecular mechanisms by which chronic bacterial insults may shape host aging and immune dysfunction.

Specifically, we frame *Mab* as a potent trigger of senescence, and establish pathogen-induced DNA damage, together with activation of the DDR, as the leading molecular architects driving macrophages towards a senescence state. We demonstrate that infection with *Mab* activates a classical DDR pathway, including phosphorylation of ATM, ATR, and DNA-PK, accumulation of γH2A.X and 53BP1 foci, and the emergence of double-strand DNA breaks (as confirmed via Comet assay). This cascade of events shapes a senescence-associated transcriptional reprogramming that involves morphological remodelling, a stable proliferative arrest and lysosomal activation (p21, SA-β-gal). The precise bacterial molecule(s) responsible for inducing host DNA damage still remain to be elucidated. In other pathogens, dedicated genotoxins have been identified. Typhoid toxin of *Salmonella Typhi* induces DNA replication stress and triggers senescence that propagates via SASP factors[40,41], while colibactin from *E. coli* strains generates DNA crosslinks leading to genomic instability[42]. No analogous genotoxin has been characterised in mycobacteria. The underlying mechanism may involve indirect pathways, including ROS/RNS-mediated oxidative damage from the sustained respiratory burst, mitochondrial dysfunction with cytosolic DNA release and cGAS-STING activation, or secreted effector molecules. Defining the exact molecular trigger represents an important direction for future work. Nonetheless, the results here reported represent a pivotal advance beyond prior observations, as we definitively linked chronic bacterial infection to classical stress-induced senescence at molecular level.

Importantly, data indicate that senescence is not confined uniquely to *Mab* infected macrophages. Conditioned media from MPI chronically exposed to *Mab* is sufficient to induce senescence features in neighbouring, uninfected macrophages, indicating a potent paracrine effect mediated by SASP. This “spread” of senescence mirrors the phenomena described in oncogenic and fibrotic contexts, and underscores a potential self-propagating feature of senescence signalling[35,36].

Unlike transient LPS-driven inflammation, or acute inflammatory responses that resolve upon pathogen clearance, *Mab* induces a sustained and progressive SASP signature detectable after five days of continuous exposure. This highlights a fundamentally different immune phenotype, suggesting that senescence can contribute to the establishment of a long-term, pro-inflammatory, niche. Our hypothesis

is that such niche might represent a successfully evolved strategy for promoting bacterial colonisation and tissue damage, thus contributing to the spread of infection. Indeed, a particularly translationally relevant aspect of our study is the demonstration that senescent macrophages are more permissive to intracellular bacterial colonisation. We are genuinely convinced that such a postulated hypothesis deserves future research efforts, as it will contribute to writing a new chapter in fields like ageing-related infections. On one hand, our data imply that senescence may serve as a host attempt to contain infection by arresting the proliferation of infected cells. On the other hand, its downstream effect, specifically SASP secretion, may paradoxically facilitate the formation of a pathogenic reservoir for future infections. This aligns with the possibility that chronic inflammation and senescence are not merely collateral damage but, instead, can be host strategies that pathogens exploit and finely manipulate for their own benefit.

Therapeutically, senolytic treatment with the Bcl-2 family inhibitor navitoclax cleared senescent macrophages and significantly reduced intracellular bacterial load without promoting extracellular bacterial dissemination. This dual action distinguishes senolytics from conventional antimicrobial therapies. Whereas antibiotics directly target bacteria, senolytics eliminate the host cell niche itself, thereby removing the protective environment that may promote bacterial survival. The senolytic efficacy extended to both primary infected and secondary bystander senescent macrophages, suggesting that elimination of the paracrine SASP loop may disrupt the self-propagating inflammatory network.

We validated the onset of cellular senescence in a physiologically relevant context using a murine model of chronic *Mab* infection. Spatial transcriptomic and classical immunohistochemistry analysis confirmed that the senescence-associated transcriptional signature was predominantly enriched in granuloma-like structures associated with chronic inflammation and correlated with the spatial localisation of *Mab*. This demonstrates that senescence pathways are activated *in vivo* at sites of persistent infection.

We further demonstrated that navitoclax treatment in chronically infected mice reduced pulmonary bacterial load. Notably, *in vivo* responses to navitoclax were heterogeneous, with animals segregating into distinct responder and mildly-responder subgroups. We hypothesise that this heterogeneity reflects differences in the relative distribution between intracellular and extracellular bacteria in this infection model. Animals with predominantly intracellular infection (higher senescent cell burden) would be expected to respond favourably to senolytic therapy, whereas those with predominantly extracellular bacteria would show a limited response, as navitoclax targets the host cell rather than free bacteria. This interpretation corroborates our *in vitro* findings, which demonstrate that navitoclax eliminates intracellular but not extracellular bacteria.

Senolytics represent a potential therapeutic window. Following standard antibiotic treatment, to reduce extracellular bacterial burden, the senolytic intervention could focus on eliminating the reservoir of infected senescent cells and dismantle the pro-inflammatory niche that sustains chronic infection. This approach could prevent bacterial reactivation while allowing tissue resolution and repair.

In conclusion, our study identifies host-cell senescence as a critical outcome of chronic *Mab* infection and establishes a mechanistic framework where pathogen-induced DNA damage, and sustained SASP signalling, converge to support bacterial survival. By targeting the senescent cell population, senolytic strategies provide a novel, host-directed therapeutic approach that can complement existing antimicrobial regimens, and may be particularly valuable in the context of rising antimicrobial resistance. The molecular framework we establish raises the possibility that other pathogens with chronic intracellular tropism (e.g., *Brucella*, *Salmonella*, and *Listeria*) might similarly exploit host DNA damage pathways to induce senescence and manipulate host tissue environments, an underexplored mechanism with far-reaching implications.

More broadly, our findings open new avenues for investigating the role of senescence across chronic infectious diseases, and for rethinking host-pathogen interactions in the frame of an evolutionary arms race where pathogens co-opt cellular senescence to establish persistent, immune-privileged niches.

Material and methods

Cells: Murine alveolar-like macrophages. Max Plank Institute (MPI) cells (alveolar-like macrophages) were cultured in RPMI 1640 medium supplemented with 10% heat-inactivated Fetal Bovine Serum, 1% Glutamine, 1% Penicillin and Streptomycin, 20 mM HEPES and 0,6 µg/mL of GM-CSF. Cell cultures were maintained in the incubator at 37°C with 5% CO_2. Cells were split twice a week and plated at 2 x 10^5 cells/mL to avoid confluence. MPI from p8 to p50 were used. Cells were routinely screened for mycoplasma contamination. For chronic LPS stimulation, media containing LPS was replaced daily, for up to 5 days.

Hela. Cells were cultured in DMEM medium supplemented with 10% heat-inactivated Fetal Bovine Serum, 1% Glutamine, 1% Penicillin and Streptomycin. Cell cultures were maintained in the incubator at 37°C with 5% CO_2. Cells were split twice a week to avoid confluency.

Peripheral blood monocytes (PBMC) . Peripheral blood was collected from healthy donors via venepuncture, following ethical approval from the Fondazione I.R.C.C.S. Ca' Granda Ospedale Maggiore Policlinico ethical committee in Milan, Italy. No personal identifying information from the donors was disclosed to the research laboratory. Human PBMCs were isolated within 24 hours of blood collection using Ficoll-Hypaque density gradient centrifugation (Amersham Pharmacia Biotech). Then monocytes were purified from the PBMCs using CD14+ magnetic microbeads (Miltenyi Biotec), in accordance with the manufacturer's instructions. The isolated CD14+ cells were then resuspended in RPMI 1640 medium supplemented with 10% fetal bovine serum (FBS), 1% Penicillin/Streptomycin, 1% Sodium Pyruvate, and 100 ng/mL human recombinant macrophage colony-stimulating factor (hM-CSF, Peprotech), which facilitates monocyte adhesion and differentiation into macrophages. After 6 days of culture, monocytes were differentiated into M0 monocyte-derived macrophages (MDMs) using 50 ng/mL M-CSF for 48 hours.

Mycobacterium abscessus Tdtomato fluorescent reporter strain. *Mycobacterium abscessus* (Mab) strains were culture at 37°C in Middlebrook 7H9 broth supplemented with 10% OADC, 0.5% glycerol and 0.05% Tween-80. Middlebrook 7H10 agar has been enriched with 10% OADC and 0.5% glycerol. Exponentially growing culture were started from a single colony, aliquots were enriched with 15% glycerol, stored at -80°C, and used to start primary cultures. Mab was grown in Middlebrook 7H9 broth at 37°C in shaking condition (150 rpm) to mid-log phase (OD600 0.5-0.8) before infection. The selective antibiotics was added for strains carrying chromosomal integrative vectors in the primary culture and removed in the secondary culture used for the final experiments. Constitutive reporter strains used in the following study were generated using the integrative vector pTdTomato-L5 (Addgene #140994). The chromosomal integration was done via the L5 phage site attB,68 Mab was transformed with the construct by electroporation (2500 V, 25 µF, 1000 Ω, 2 mm path) and plated on Middlebrook 7H10 agar containing Streptomycin at a concentration of 30 µg/mL. For the infection, MPI cells were plated at $2x10^5$ cells/mL one day in advance, then infected at the indicated MOI (1:0.25 or 1:0.5) for 2 hours, finally washed with PBS three times and incubated at 37°C 5% CO_2. To obtain a model for chronic infection and to avoid cell death due to the extracellular growth of *Mab*, the medium was replaced daily from day 3 post-infection. To produce the inactivated form of the pathogen, *Mab* culture was centrifuged for 15 minutes at 15,000g. The pellet was resuspended in 0.3% (v/v) of beta-propiolactone in sterilized water and incubated at 4°C for 24 hours to allow pathogen inactivation without damaging its structure. The sample was transferred at 37°C for 2 hours, then washed 3 times with PBS.

RNA isolation and analysis. MPI (infected or uninfected) were cultured up to 5 days, then detached with trypsin and pelleted. Samples were prepared according to the Maxwell RSC simplyRNA Cells Kit (#AS1390) and loaded onto Maxwell® RSC Cartridges for automated RNA extraction, which was performed on Maxwell Instrument. Extracted RNA was quantified with Thermo Scientific™ NanoDrop™ One/OneC Microvolume UV-Vis Spectrophotometer. For RNA-seq, 2µg poly-A RNA for each sample was subjected to subsequent quality control, library construction and high-throughput sequencing at Eurofins Genomics. A paired end (2 × 150) run was performed on illumina NovaSeq.

RNASeq bioinformatics analysis. After initial quality check, the reads were mapped on mouse reference genome GRCm39 with STAR mapping software (v.2.7.11a)[43]. To estimate differential expression, the matrix of gene counts for each sample produced by STAR with parameter "--quantMode GeneCounts" was analysed in R with the library DESeq2 (v.1.48.0)[44]. Differential expression analysis was performed for the selected comparisons (*i.e. Mab* exposed d1 vs Uninfected d1, *Mab* exposed d5 vs Uninfected d5, *Mab* exposed d5 vs *Mab* exposed d1, *Mab* exposed d5 vs Uninfected d1). Genes with an absolute value of log2(fold change) higher than 1 and FDR lower than 0.05 were considered significantly differentially expressed between the two conditions. Gene expression levels between treatment groups were further analysed for their pathway enrichments using gene set enrichment analysis (GSEA). GSEA was performed in R with the package fgsea (v.1.30.0)[45] on the m5 GO Biological Process ontology obtained from MSigDB[46]and on selected senescence related pathways, such as SAUL SenMayo[28], or SenePy[47].

Genes were ranked based on their shrinkage-adjusted log2 fold change and used as input for GSEA analysis. Gene set pathway networks were generated using the aPEAR package (v.1.0.0)[48].

To assess the specific effects on SASP-associated genes, we filtered the GSEA networks derived from the m5 BP ontology to retain only gene sets containing at least one SASP gene. To compare SASP gene expression between acute (1-day) and chronic (5-day) infection, we further refined the selection by including only gene sets containing at least one of the following immune- or inflammation-related keywords:

Keywords			
interferon	viral	virus	antiviral
cytokine	chemokine	interleukin	tnf
chemotaxis	migration	recruitment	immune
inflammatory	inflammation	complement	antibody
antigen	immunoglobulin	leukocyte	macrophage
monocyte	lymphocyte	collagen	matrix
ecm	extracellular	peptidase	protease
metalloproteinase	remodeling	tissue	degradation
fibrin	coagulation	hemostasis	plasminogen
prostaglandin	lipid	fatty_acid	secretion
transport	exocytosis	tlr	toll_like
lps	lipopolysaccharide	pattern_recognition	innate_immune
nf_kappa	nfkb	kappa_b	defense
response_to_bacterium	response_to_pathogen	cell_cycle	mitot
meiotic	chromosome	chromatid	dna_replication
kinetochore	centrosome	spindle	cytokinesis
cell_division	g1_s	g2_m	s_phase
m_phase	dna_synthesis	dna_repair	nucleotide_biosynthesis
ribosome_biogenesis			

EdU staining. To assess cell proliferation upon chronic infection, EdU fluorescent staining was performed using Click-it EdU cell proliferation kit (Thermo Scientific). Cells were labelled with EdU (5-ethynyl-2´-deoxyuridine) (10 μM) for 1 hour then fixed with 4% (v/v) paraformaldehyde (PFA) in PBS for

15 minutes. Cell permeabilization was performed using 0.5% (v/v) Triton X-100 in PBS. For detection, Click-it reaction, containing AlexaFluor-647 fluorophore, was prepared following manufacturer instructions. After 30 minutes of incubation, protected from light, cells were washed with 3% (v/v) Bovine serum albumin (BSA) in PBS. Additional staining was performed for nuclei visualisation using Hoechst 1:500 in PBS (Cell Signaling) for 15 minutes. Cells were maintained in PBS at 4°C until the analysis.

Antibodies. The followed antibodies were used for immunostaining: Waf1/Cip1/CDKN1A p21 (Santa Cruz, sc-6246, 1:200), anti-phospho-histone H2A.X (γH2AX) (Cell Signaling, #2577, 1:500); anti-53BP1 antibody (Abcam, ab175933, 1:200); Anti-ATR (phospho T1989) (Abcam, ab289363, 1:500); anti-phospho-ATM (Ser1981) (Merk, 05-740, 1:500); anti-DNA PKcs (phospho S2056) (Abcam, ab18192, 1:500); anti-Ki-67 (ThermoFisher, MA5-14520, 1:200); Alexa Fluor® 488 goat anti-rabbit IgG (Invitrogen, A1034, 1:500); Alexa Fluor® 488-Goat anti-mouse IgG (Thermo Scientific. 1:500).

Immunofluorescence. Cells were fixed with 4% (v/v) PFA for 20 minutes, washed twice in PBS, permeabilised with 0.5% (v/v) Triton™ X-100 for 10 minutes and blocked with 5% (v/v) BSA for 1 hour at room temperature. Cells were incubated with primary antibody in 1% (v/v) BSA in PBS for 1h at room temperature or overnight at 4°C. After 3 washes with PBS, cells were incubated with secondary antibody for 1 hour at room temperature. Finally, nuclei were counterstained with Hoechst (Cell Signalling. 1:500 in PBS) and cell membranes with CellMask™ Deep Red Plasma membrane (Thermo Scientific. 1:1000 in PBS). After 15 minutes of incubation, cells were washed with PBS and stored at 4°C until analysis.

Live-cell imaging*:* Cells were stained with Hoechst 33342 (Cell Signalling. 1:500 in RPMI) and CellMask™ Deep Red Plasma membrane (Thermo Scientific. 1:1000 in RPMI) for 20 minutes at 37°C then washed once in PBS. For SA-b-gal analysis, cells were pre-treated with Bafilomycin A1 (MedChemExpress, HY-100558,) 100 nM for 1 hour, then stained with C12FDG (Abcam, ab273642) 33μM for 45 minutes at 37°C. Cells were then fixed with 4% (v/v) PFA for 20 minutes and stored in PBS at 4°C until analysis. For apoptosis visualisation, BioTracker NucView® 488 Green Caspase-3 Dye (Merk, SCT101) 5μM was added to the medium before live imaging microscopy up to 24h.

High-resolution confocal microscopy. Fluorescence staining was visualised cusing Leica STELLARIS 8 Confocal microscopy with LasX software (Leica). For every sample, 10-60 fields of view with 20x or 40x magnification objectives were acquired, for a total of up to 4000 cells per condition. Quantitative microscopy analysis was performed using NIS-Elements Advanced Research (Nikon) software or CellProfiler 4.2.7. The logical features analysed were extracted using CellProfiler 4.2.7 and are in Table 2.

Comet Assay. For both neutral and alkaline comet assay, cells were detached with trypsin, pelleted and resuspended in PBS. Samples were prepared following CometAssay® Kit (Bio-Techne #4250-050-K) instructions. Comet's tail moment was quantified using TriTek CometSCore 2.0.0.38.

Conditioned media. Conditioned media was collected on the fifth-day post-infection (MOI 1:0.25), centrifuged at 1800 rcf, and the supernatant was filtered using a 0.22 μm syringe filter. Several dilutions

were performed adding RPMI to the filtered media and supplemented with 0,6 µg/mL of GM-CSF. Healthy MPI were then exposed to different concentrations of conditioned media for up to 72 hours, changing the media daily. Cells were then stained with C12FGD and analysed through confocal microscopy.

Quantitative PCR with reverse transcription. Total RNA was extracted from murine and human cells following the manufacturer's instructions on Monarch® Total RNA Miniprep Kit (T2010S, New England Biolabs). Extracted RNA was quantified with Thermo Scientific™ NanoDrop™ One/OneC Microvolume UV-Vis Spectrophotometer. The reverse transcription was performed with ProtoScript® II First Strand cDNA Synthesis Kit (E6560S, New England Biolabs) using the optimised Random Primer Mix provided by the manufacturer. cDNA produced was diluted in nuclease-free water and 5ng were added in each well of a 96-well plate where the forward and reverse primers for the gene of interest and SensiFAST™ SYBR® Lo-ROX Kit (BIO-94020, Meridian Bioscience) were mixed. The RT-qPCR was performed using a Quant Studio Real Time PCR System (Thermo Scientific), all the samples were measured in technical triplicates and the curves of amplification were analysed with Design and Analysis Software Version 2.6 (Thermo Scientific). Expression data were normalised to *Rps18* gene. Fold change was calculated using the $2^{-\Delta\Delta Ct}$ method. All primer sequences were reported in the Supplementary Tab.

ELISA. The supernatants derived from uninfected, *Mab*-exposed cells or LPS treatments (10-1000 ng/ml) were harvested and stored at -80°C. Assessment of TNFα, IL6 and IL10 production was performed using a commercially available kit (BioLegend), following the manufacturer's protocols. (TNFα: 430904, IL6: 431304, IL10: 431414).

Senolytic and antibiotic treatment *in vitro*. Amikacin (MCE, HY-B0509A) was added to the medium on the fourth day of infection at 250 µg/ml for 2 hours, then a maintenance dose of 50 µg/ml was left overnight. On the fifth day of infection, the media was changed and cells were treated with navitoclax (MCE, HY-10087) 4µM or Amikacin 50µg/ml for 24h.

CFU assay. Upon antibiotic and senolytic treatments, both the medium and the cells were collected to assess the number of extra and intracellular bacteria. For intracellular bacteria assessment 0.5% (v/v) SDS in PBS was used to lyse cells, while for extracellular bacteria the medium was collected and centrifuged at 400rcf for 5 minutes, then the pellet resuspended in PBS. 1:20 serial dilutions were performed in PBS before spreading the diluted samples onto Middlebrook 7H10 agar base (Sigma) plates. After 5 days of incubation, CFU were counted.

Mouse models of *Mab* infection and *in vivo* treatments. C57BL/6N mice were maintained in specific pathogen free conditions at the animal house of the San Raffaele Scientific Institute (Milan, Italy). Animal experiments in this study were performed according to protocols approved by the San Raffaele Scientific Institute Animal Care and Use Committee (IACUC) in full agreement with the Italian legislation and after authorisation by the Italian Ministry of Health (IACUC protocol number#1242). We used an in-house developed agar beads mouse model of respiratory infection by *Mab* in the immunocompetent C57BL/6N murine genetic background[38,39,49]. Mice were then infected with an intratracheal injection of 10^5 CFU of

Mab, which allows long-term bacterial persistence in the lung. Following infection, mice were monitored daily for body weight variation and were sacrificed at 21 days after infection for lung collection. For the pharmacological treatment, starting from day 7 post infection, mice were treated daily for 2 weeks with vehicle (saline solution), Amikacin (intraperitoneal administration: 100 mg/kg, as positive control group) and Navitoclax (oral gavage: 50 mg/kg). At the end of treatment (14 days post challenge), the mice were euthanised, and their lungs were excised aseptically and homogenised in 2 mL PBS using the homogenizer gentleMACSTM Octo Dissociator. Bacterial loads in local (lung homogenates) compartments were determined by plating the samples at 10-fold serial dilution in 7H10 agar medium (Difco; Becton Dickinson, Franklin Lakes, NJ, USA). The experiment was repeated twice.

Spatial transcriptomics. For spatial transcriptomics analysis, we exploited a previous study related to dual spatial host-bacterial gene expression in Mycobacterium abscessus respiratory infections. The published dataset[50] was exploited (GEO under accession number GSE242471) to assess gene expression related to senescence in this work.

Dual spatial host-bacterial gene expression was performed using the 10x Visium technology. Formalin-fixed paraffin-embedded (FFPE) tissues were sectioned at 5 µm in thickness and attached to a Visium Spatial Gene expression slide and processed as previously described. Detailed description of sample, data processing and computational analyses can be found in the original manuscript[50].

Clustering annotation was adopted from the original publication. Principal components were used to generate a revised 2-dimensional Uniform Manifold Approximation and Projection (UMAP) for visualisation (with 30 nearest neighbours). The genes representing the senescent gene signature were identified in previous publications[28]. The expression of the Senescent gene signature was determined in the annotated clusters. Moreover, spots demonstrating at least one read for the custom probe were designated as *Mab* (*Mab*$^{+}$). The expression of Senescent gene signature was evaluated in *Mab*$^{+}$ spots from *Mab*$^{-}$ spots were obtained using 'FindMarkers' in Seurat, with default settings on the SCT normalized matrix. A nonparametric two-tailed Mann–Whitney U test was performed for the analysis.

Histological analysis. Lungs were removed and fixed in 4% paraformaldehyde. After paraffin embedding, consecutive 5-µm sections from the middle of the five lung lobes were used for histological and immunohistochemical examination. Sections were stained, as previously described, with haematoxylin and eosin (H&E) or with anti-p21 antibodies[50,51]. Images were acquired using the Aperio CS2 scanner (Leica Biosystems, Nussloch, Germany) and analysed with the Aperio ImageScope software (Leica Biosystems).

Statistical analysis. GraphPad Prism Software Version 10 was used for statistical analyses. Two-tailed Student's t-tests to compare two experimental groups; otherwise, for more groups one-way ANOVA with Tukey's multiple comparison test was performed. Nonparametric Kruskal-Wallis or Kolmogorov-Smirnov

tests were performed for nonnormally distributed data. For the *in vivo* lung CFUs experiment, outliers were identified using the ROUT method with Q = 0.5%. Data handling was performed using Spyder 5.5.1 on Anaconda Navigator 2.5.2.

Table.1: Primers list:

Rps18	Forward: CGGAAAATAGCCTTCGCCATCAC
	Reverse: ATCACTCGCTCCACCTCATCCT
Ccnd1	Forward: GCTGTGCATCTA CACCGACA
	Reverse: TTGAGCTTGTTCA CCAGGAG
Il1a	Forward: CGCTTGAGTCGGCA AAGAAAT
	Reverse: TGGCAGAACTGTAG TCTTCGT
Il1b	Forward: TGGACCTTCCAGGATGAGG ACA
	Reverse: GTTCATCTCGGAGCCTGTA GTG
Il6	Forward: TACCACTTCACAAGTCGGA GGC
	Reverse: CTGCAAGTGCATCATCGTT GTTC
Il10	Forward: CGGGAAGACAATAACTGCA CCC
	Reverse: CGGTTAGCAGTATGTTGTC CAGC
Lmnb1	Forward: GTGCTGCGAGCA GGAGAC
	Reverse: CCATTAAGATCAG ATTCCTTCTTAGC
Mmp2	Forward: CTCTGCGTCCTGTG CTGCCTGTTG
	Reverse: AAAGTGAGAATCTCC CCCAACACC
Cdkn2a	Forward: GAACTCTTTCGGTC GTACCC
	Reverse: CGAATCTGCACCGT AGTTGA
Cdkn1a	Forward: TCCCGACTCTTGAC ATTGCT
	Reverse: TGCAGAAGGGGAAG TATGGG
Trp53	Forward: TAGGTAGCGACTACAGTTAGGG
	Reverse: CATGGCAGTCATCCAGTCTT
Tnfa	Forward: GGTGCCTATGTCTCAGCCT CTT
	Reverse: GCCATAGAACTGATGAGAG GGAG

Table. 2: Morphological features

AreaShape_Area	AreaShape_BoundingBoxArea
AreaShape_BoundingBoxMaximum_X	AreaShape_BoundingBoxMaximum_Y
AreaShape_BoundingBoxMinimum_X	AreaShape_BoundingBoxMinimum_Y
AreaShape_Center_X	AreaShape_Center_Y
AreaShape_CentralMoment_0_1	AreaShape_Compactness
AreaShape_ConvexArea	AreaShape_Eccentricity
AreaShape_EquivalentDiameter	AreaShape_EulerNumber
AreaShape_Extent	AreaShape_FormFactor
AreaShape_HuMoment_0	AreaShape_InertiaTensorEigenvalues_0
AreaShape_InertiaTensor_1_1	AreaShape_MajorAxisLength
AreaShape_MaxFeretDiameter	AreaShape_MaximumRadius
AreaShape_MeanRadius	AreaShape_MedianRadius
AreaShape_MinFeretDiameter	AreaShape_MinorAxisLength
AreaShape_NormalizedMoment_0_0	AreaShape_NormalizedMoment_0_1
AreaShape_NormalizedMoment_1_0	AreaShape_Orientation
AreaShape_Perimeter	AreaShape_Solidity
AreaShape_SpatialMoment_1_0	

Declarations

Acknowledgments

The authors acknowledge the scientific and technical assistance of Dr. Mariacristina Crosti of the Sorting Facility in INGM and Dr Chiara Cordiglieri of the Imaging Facility in INGM. We thank Professor Marina Freuderberg (BIOOS Centre for Biological Signaling Studies, University of Freiburg) for kindly providing MPI-2 cells. This work was funded by grants to L.R. from ERC-2019-STG (grant number 850936), Fondazione Cariplo (grant number 2019-4278), E.S Fondazione Cariplo (grant number 2022-0438) and the Italian Ministry of University and Research (grant number FIS-2023-00860, DD n. 22831 del 5/12/2024 BANDO FIS 2), Linea 4 University of Milan (PSRL423ESCAR_0). This study has also been funded by a grant 2025 from the European Society of Clinical Microbiology and Infectious Disease (Europäische Gesellschaft für klinische Mikrobiologie und Infektionskrankheiten) (ESCMID) to A.G.

Contributions

Conceptualisation: E.S., L.R. Methodology D.O., E.S., D.R., C.C., F.R., R.N, G.M., M.A., L.M., D.M.C., S.A., R.D.M., N.I.L., L.R. Formal Analysis. D.O., E.S., D.R., C.C., F.R., R.N, F.D.M., F.S., G.M., M.A., L.M., N.I.L., L.R. Resources. D.O., E.S., D.R., C.C., F.R., R.N, G.M., A.G., A.V., M.Z., F.D.M., F.S., G.M., F.C., G.C., L.M., Writing – Original draft D.O., E.S., D.R., N.I.L., L.R. Writing - Review & Editing D.O., E.S., D.R., F.C., M.A., G.C., D.M.C., R.D.F., S.A., R.D.M., N.I.L., L.R. Visualisation D.O., E.S., D.R., N.I.L., L.R. Supervision E.S., N.I.L., L.R. Project administration E.S., L.R. Funding acquisition: E.S, L.R.

Competing interests

The authors declare no competing interests.

References

1. Fumagalli, M. *et al.* Signatures of environmental genetic adaptation pinpoint pathogens as the main selective pressure through human evolution. *PLoS Genet* 7, (2011).
2. Sironi, M., Cagliani, R., Forni, D. & Clerici, M. Evolutionary insights into host-pathogen interactions from mammalian sequence data. *Nature Reviews Genetics* vol. 16 224–236 (2015).
3. Walsh, D. P., Felts, B. L., Cassirer, E. F., Besser, T. E. & Jenks, J. A. Host vs. pathogen evolutionary arms race: Effects of exposure history on individual response to a genetically diverse pathogen. *Front Ecol Evol* 10, (2023).
4. Chi, H., Pepper, M. & Thomas, P. G. Principles and therapeutic applications of adaptive immunity. *Cell* vol. 187 2052–2078 (2024).
5. Finlay, B. B. & McFadden, G. Anti-immunology: Evasion of the host immune system by bacterial and viral pathogens. *Cell* vol. 124 767–782 (2006).
6. Toyofuku, M., Schild, S., Kaparakis-Liaskos, M. & Eberl, L. Composition and functions of bacterial membrane vesicles. *Nature Reviews Microbiology* vol. 21 415–430 (2023).
7. Sanchez-Garrido, J., Ruano-Gallego, D., Choudhary, J. S. & Frankel, G. The type III secretion system effector network hypothesis. *Trends in Microbiology* vol. 30 524–533 (2022).
8. Casadevall, A. & Pirofski, L. A. The damage-response framework of microbial pathogenesis. *Nat Rev Microbiol* 1, 17–24 (2003).
9. Remick, B. C., Gaidt, M. M. & Vance, R. E. Effector-Triggered Immunity. *Annu Rev Immunol* 41, 453–481 (2023).
10. Nie, J. *et al.* Deep insight into cytokine storm: from pathogenesis to treatment. *Signal Transduction and Targeted Therapy* vol. 10 (2025).
11. López-Otín, C., Blasco, M. A., Partridge, L., Serrano, M. & Kroemer, G. Hallmarks of aging: An expanding universe. *Cell* vol. 186 243–278 (2023).
12. Gorgoulis, V. *et al.* Cellular Senescence: Defining a Path Forward. *Cell* vol. 179 813–827 (2019).

13. Wang, B., Han, J., Elisseeff, J. H. & Demaria, M. The senescence-associated secretory phenotype and its physiological and pathological implications. *Nature Reviews Molecular Cell Biology* vol. 25 958–978 (2024).
14. Di Micco, R., Krizhanovsky, V., Baker, D. & d'Adda di Fagagna, F. Cellular senescence in ageing: from mechanisms to therapeutic opportunities. *Nat Rev Mol Cell Biol* 22, 75–95 (2021).
15. Reyes, A. *et al.* Contribution of viral and bacterial infections to senescence and immunosenescence. *Frontiers in Cellular and Infection Microbiology* vol. 13 (2023).
16. Zheng, S. yu *et al.* Helicobacter pylori-positive chronic atrophic gastritis and cellular senescence. *Helicobacter* vol. 28 (2023).
17. Lee, S. *et al.* Correction to: Virus-induced senescence is a driver and therapeutic target in COVID-19 (Nature, (2021), 599, 7884, (283-289). *Nature* vol. 638 E46 (2025).
18. Kohli, J., Veenstra, I. & Demaria, M. The struggle of a good friend getting old: cellular senescence in viral responses and therapy. *EMBO Rep* 22, (2021).
19. Delval, L. *et al.* Removal of senescent cells reduces the viral load and attenuates pulmonary and systemic inflammation in SARS-CoV-2-infected, aged hamsters. *Nat Aging* 3, 829–845 (2023).
20. Chen, H. Y. *et al.* Mitochondrial injury induced by a Salmonella genotoxin triggers the proinflammatory senescence-associated secretory phenotype. *Nat Commun* 15, (2024).
21. Zhang, J. *et al.* Bacterial pneumonia induces senescence in resident alveolar macrophages that are outcompeted by monocytes. *Cell Rep* 44, (2025).
22. Sun, G. *et al.* A single-cell transcriptomic atlas reveals senescence and inflammation in the post-tuberculosis human lung. *Nat Microbiol* 10, 2073–2091 (2025).
23. Johansen, M. D., Herrmann, J. L. & Kremer, L. Non-tuberculous mycobacteria and the rise of Mycobacterium abscessus. *Nature Reviews Microbiology* vol. 18 392–407 (2020).
24. Meliefste, H. M., Mudde, S. E., Ammerman, N. C., de Steenwinkel, J. E. M. & Bax, H. I. A laboratory perspective on Mycobacterium abscessus biofilm culture, characterization and drug activity testing. *Frontiers in Microbiology* vol. 15 (2024).
25. Woo, M. *et al.* Mycobacterium tuberculosis Infection and Innate Responses in a New Model of Lung Alveolar Macrophages. *Front Immunol* 9, (2018).
26. Fejer, G. *et al.* Nontransformed, GM-CSF-dependent macrophage lines are a unique model to study tissue macrophage functions. *Proc Natl Acad Sci U S A* 110, E2191–E2198 (2013).
27. Duran, I., Bishop, C. L., Gil, J. & Wallis, R. The promise of machine learning approaches to capture cellular senescence heterogeneity. *Nat Aging* 4, 1167–1170 (2024).
28. Saul, D. *et al.* A new gene set identifies senescent cells and predicts senescence-associated pathways across tissues. *Nat Commun* 13, 4827 (2022).
29. Kohli, J. *et al. Algorithmic Assessment of Cellular Senescence in Experimental and Clinical Specimens*. *Nature Protocols* vol. 16 (Springer US, 2021).
30. Gorgoulis, V. *et al.* Cellular Senescence: Defining a Path Forward. *Cell* 179, 813–827 (2019).

31. Debacq-Chainiaux, F., Erusalimsky, J. D., Campisi, J. & Toussaint, O. Protocols to detect senescence-associated beta-galactosidase (SA-βgal) activity, a biomarker of senescent cells in culture and in vivo. *Nat Protoc* 4, 1798–1806 (2009).
32. Shen, W. *et al.* Senescent macrophages in tumor: phenotypes, roles, and interventions. *Cell Death Dis* 16, 677 (2025).
33. Sanborn, M. A., Wang, X., Gao, S., Dai, Y. & Rehman, J. Unveiling the cell-type-specific landscape of cellular senescence through single-cell transcriptomics using SenePy. *Nature Communications* 16, (2025).
34. Wang, B., Han, J., Elisseeff, J. H. & Demaria, M. The senescence-associated secretory phenotype and its physiological and pathological implications. *Nat Rev Mol Cell Biol* 25, 958–978 (2024).
35. Acosta, J. C. *et al.* A complex secretory program orchestrated by the inflammasome controls paracrine senescence. *Nat Cell Biol* 15, 978–990 (2013).
36. Ortiz-Montero, P., Londoño-Vallejo, A. & Vernot, J.-P. Senescence-associated IL-6 and IL-8 cytokines induce a self- and cross-reinforced senescence/inflammatory milieu strengthening tumorigenic capabilities in the MCF-7 breast cancer cell line. *Cell Communication and Signaling* 15, 17 (2017).
37. Sogabe, Y. *et al.* Characterizing primary and secondary senescence in vivo. *Nat Aging* 5, 1568–1588 (2025).
38. Lorè, N. I. *et al.* The aminoglycoside-modifying enzyme Eis2 represents a new potential in vivo target for reducing antimicrobial drug resistance in Mycobacterium abscessus complex. *European Respiratory Journal* 60, (2022).
39. Riva, C. *et al.* A new model of chronic mycobacterium abscessus lung infection in immunocompetent mice. *Int J Mol Sci* 21, 1–12 (2020).
40. Chen, H.-Y. *et al.* Mitochondrial injury induced by a Salmonella genotoxin triggers the proinflammatory senescence-associated secretory phenotype. *Nat Commun* 15, 2778 (2024).
41. Ibler, A. E. M. *et al.* Typhoid toxin exhausts the RPA response to DNA replication stress driving senescence and Salmonella infection. *Nat Commun* 10, (2019).
42. Dziubańska-Kusibab, P. J. *et al.* Colibactin DNA-damage signature indicates mutational impact in colorectal cancer. *Nat Med* 26, 1063–1069 (2020).
43. Dobin, A. *et al.* STAR: Ultrafast universal RNA-seq aligner. *Bioinformatics* 29, 15–21 (2013).
44. Love, M. I., Huber, W. & Anders, S. Moderated estimation of fold change and dispersion for RNA-seq data with DESeq2. *Genome Biol* 15, (2014).
45. Korotkevich, G. *et al.* Fast gene set enrichment analysis. Preprint at https://doi.org/10.1101/060012 (2016).
46. Castanza, A. S. *et al.* Extending support for mouse data in the Molecular Signatures Database (MSigDB). *Nature Methods* vol. 20 1619–1620 (2023).
47. Sanborn, M. A., Wang, X., Gao, S., Dai, Y. & Rehman, J. Unveiling the cell-type-specific landscape of cellular senescence through single-cell transcriptomics using SenePy. *Nat Commun* 16, 1884 (2025).

48. Kerseviciute, I. & Gordevicius, J. aPEAR: an R package for autonomous visualization of pathway enrichment networks. *Bioinformatics* 39, (2023).
49. Degiacomi, G. *et al.* The novel drug candidate VOMG kills Mycobacterium abscessus and other pathogens by inhibiting cell division. *Int J Antimicrob Agents* 64, (2024).
50. Di Marco, F. *et al.* Dual spatial host-bacterial gene expression in Mycobacterium abscessus respiratory infections. *Commun Biol* 7, (2024).
51. Saliu, F. *et al.* Chronic infection by nontypeable haemophilus influenzae fuels airway inflammation. *ERJ Open Res* 7, (2021).

Figures

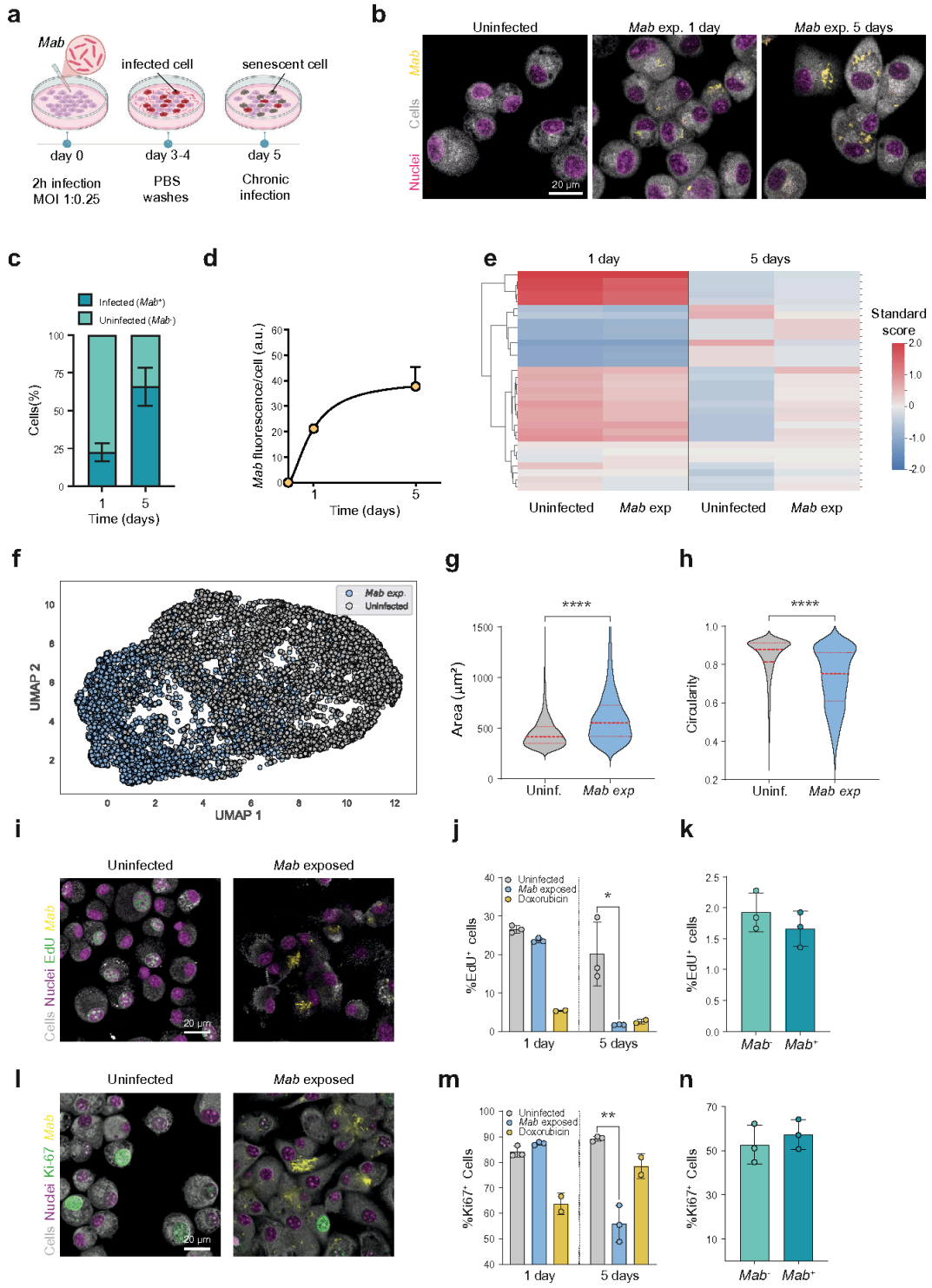


Figure 1

a, Schematic diagram of the chronic *Mycobacterium abscessus* (*Mab*) infection protocol. Infection begins on day 0 with a low multiplicity of infection (MOI) for 2 hours, followed by PBS washes and media changes on days 3 and 4 to establish chronic exposure by day 5. b, Representative immunofluorescence images of uninfected and *Mab* exposed cells. Left, uninfected controls; middle, acute exposure (day 1); right, chronic exposure (day 5). Nucleus (Hoechst, magenta), cell body (CellMask, grey), Mab (tdTom,

yellow). Scale bar, 20 µm. c, Quantification of the percentage of *Mab* infected cells (*Mab*$^{+}$) over time. d, Quantification of intracellular *Mab* fluorescence per cell over time. e, Heatmap of the standard-score profile in uninfected and *Mab* exposed cells. The y-axis comprises 32 cellular morphological features (Red = positive modulation, Blue = negative modulation, White = no change). **f,** UMAP dimensionality plot of the morphological features in uninfected (grey) and *Mab* exposed (light blue) cells. g-**h,** Violin plot of cell area (**g**), cell circularity (**h**) of uninfected and *Mab*-exposed cells at day 5. Central dashed line indicates the median; upper and lower dotted lines indicate the quartiles. Non-parametric t-test (Mann-Whitney) analysis (****p<0.0001). Data are from at least 6500 cells. **i,** Representative confocal microscope images of uninfected or *Mab*-exposed cells at day 5 stained with EdU. Cell nucleus (Hoechst, magenta), EdU (green) and *Mab* (tdTom, yellow). Scale bar 20µm. **j**, Quantification of the percentage of EdU positive cells in uninfected, *Mab* exposed cells and doxorubicin control at day 1 and 5. **k**, Quantification of the percentage of EdU positive cells in *Mab exposed* cells at day 5, differentiating between *Mab*$^{+}$ and *Mab*$^{-}$ cells. **l,** Representative confocal microscope images of uninfected or *Mab*-exposed cells at day 5 stained with Ki67. Cell nucleus (Hoechst, magenta), Ki67 (green), cell (Cellmask, grey) and *Mab* (tdTom, yellow). Scale bar 20µm. **m,** Quantification of the percentage of Ki67 positive cells in uninfected, *Mab* exposed cells and doxorubicin control at day 1 and 5. **n,** Quantification of the percentage of Ki67 positive cells in *Mab exposed* cells at day 5, differentiating between infected (*Mab*$^{+}$) and uninfected (*Mab*$^{-}$) cells. Data represent mean ± s.d. (*n* = 3 biological replicates per condition).

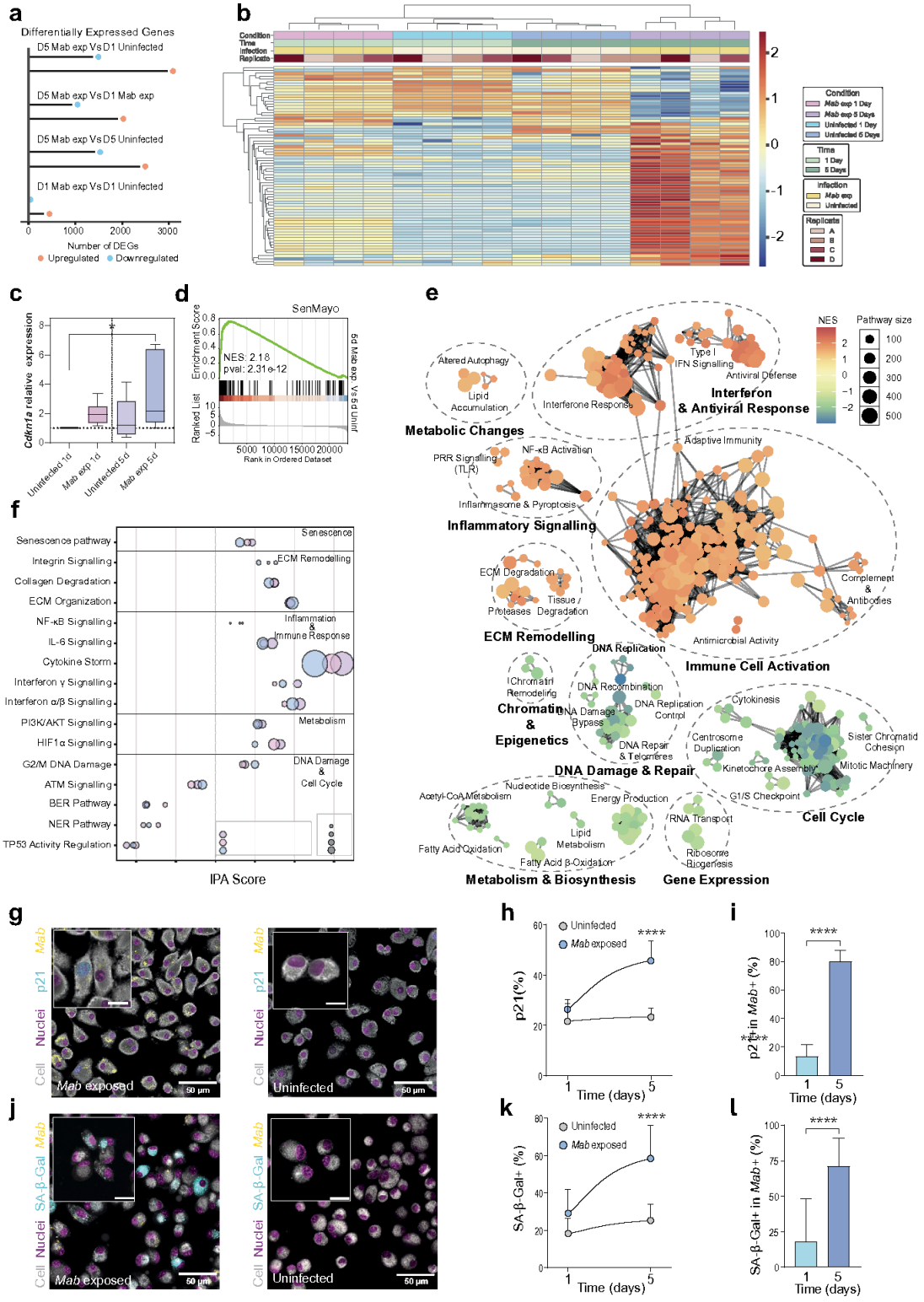


Figure 2

a, Summary representation of total number of differentially expressed genes (DEGs) for each analysed comparison. **b**, Heatmap of SenMayo gene set[28] expression across experimental conditions. Genes are hierarchically clustered by expression pattern. Colour intensity indicates z-scored normalised expression values (red, upregulated; blue, downregulated). **c**, Quantification of *Cdkn1a* across different experimental conditions. Non-parametric (Kruskal-Wallis) analysis (*p<0.05). **d**, Gene Set Enrichment Analysis (GSEA)

of the SenMayo senescence signature[28]. GSEA plot for the comparison *Mab* exposed cells (5 days) versus untreated controls (5 days), showing significant enrichment of the SenMayo gene set in *Mab* exposed cells. **e**, Integrated pathway enrichment network analysis. Network visualisation depicting relationships between enriched biological processes and pathways in *Mab* exposed senescent cells. Node size represents pathway size; node colour indicates normalised enrichment score (NES). **f**, Ingenuity pathway analysis (IPA). Horizontal bar graph showing the IPA score for various biological processes. Bubble size indicates -log10(adjusted P value). Categories: senescence, ECM remodelling, inflammation and immune response, metabolism, DNA damage and cell cycle regulation. **g**, Representative confocal microscope images of uninfected or *Mab*-exposed cells at day 5 stained for p21. Cell nucleus (Hoechst, magenta), antibody anti-p21 (cyan), cell (Cellmask, grey), and *Mab* (tdTom, yellow). Scale bar 50µm, inset scale bar 25µm. **h,** Time-dependent variation of the percentage of $p21^+$ cells. Non-parametric t-test (Mann-Whitney) analysis (**** p<0.0001). **i**, Percentage of $p21^+$ cells in Mab^+. Non-parametric t-test (Mann-Whitney) analysis (**** p<0.0001). **j**, Representative confocal microscope images of uninfected or *Mab*-exposed cells at day 5 stained for SA-β-Gal. Cell nucleus (Hoechst, magenta), SA-β-Gal (C12FDG, cyan), cell (Cellmask, grey), and *Mab* (tdTom, yellow). Scale bar 50µm, inset scale bar 25µm. **k,** Time-dependent variation of the percentage of SA-β-Gal positive cells. Non-parametric t-test (Mann-Whitney) analysis (**** p<0.0001). **l**, Percentage of SA-β-Gal^+ cells in Mab^+. Non-parametric t-test (Mann-Whitney) analysis (**** p<0.0001). Data represent mean ± s.d. (*n* = 3 biological replicates per condition).

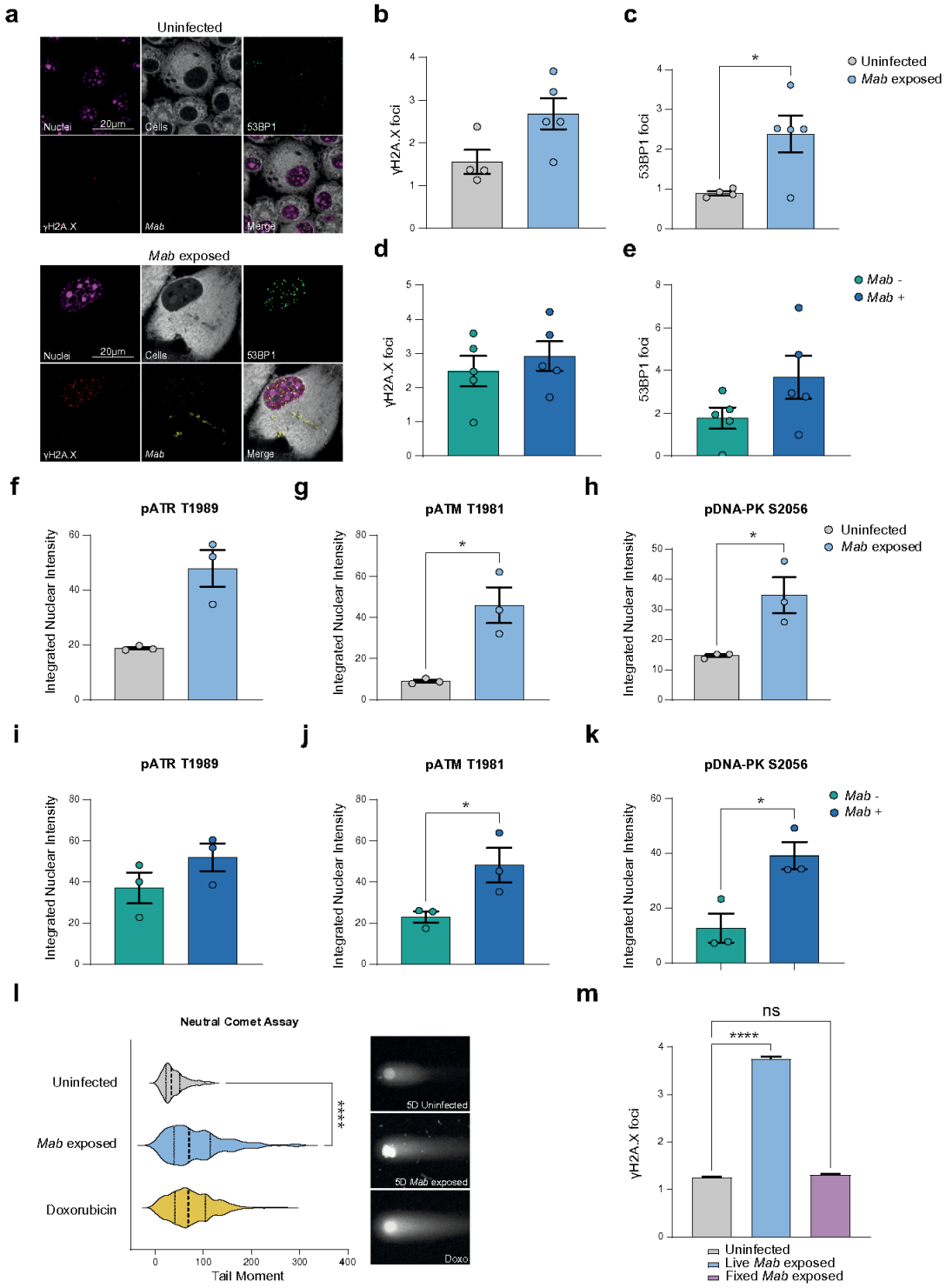


Figure 3

a, Representative immunofluorescence images of uninfected cells and *Mab* exposed cells. Top panel shows uninfected control cells; bottom panel shows cells exposed to *Mab* for 5 days. Cell nucleus (Hoechst, magenta), cell (Cellmask, grey), γH2A.X (Alexa Fluor 488, green), 53BP1 (Alexa fluor 568, red), *Mab* (tdTom, yellow). Scale bar 20µm. **b-c**, Quantification of γH2A.X (**b**) and 53BP1 (**c**) foci in uninfected and *Mab* exposed cells at 5 days. Parametric t-test (Welch's test) analysis (* p<0.05). 5 biological

replicates. **d-e.** Quantification of γH2A.X (**d**) and 53BP1 (**e**) foci in *Mab exposed* cells at day 5, differentiating between Mab^+ and Mab^- cells. Parametric t-test (Welch's test) analysis (* $p<0.05$). 5 biological replicates. **f-h.** Quantification of immunofluorescence staining using antibodies against ATR phosphorylated T1989 (**f**), ATM phosphorylated T1981 (**g**), DNA-PK phosphorylated S2056 (**h**), comparing uninfected and cells exposed to *Mab* for 5 days. Parametric t-test (Welch's test) analysis (* $p<0.05$). At least **i-k.** Quantification of immunofluorescence staining in *Mab* exposed cells, differentiating between Mab^+ and Mab^- cells, using antibodies against ATR phosphorylated T1989 (**f**), ATM phosphorylated T1981 (**g**), DNA-PK phosphorylated S2056 (**h**), comparing uninfected and cells exposed to *Mab* for 5 days. Parametric t-test (Welch's test) analysis (* $p<0.05$). **l**. Quantification of tail moments in neutral comet assay, comparing uninfected control cells, cells exposed to *Mab* for 5 days, and doxorubicin treated cells as a positive control. Representative images shown on the right. Non-parametric one-way ANOVA (Kruskal-Wallis test) analysis (**** $p<0.0001$). At least 3000 cells per condition. **m**. Quantification of γH2A.X foci comparing uninfected control cells, cells exposed to live *Mab* or propriolactone fixed *Mab* for 5 days. Non-parametric one-way ANOVA (Kruskal-Wallis test) analysis (**** $p<0.0001$). At least 3000 cells per condition.

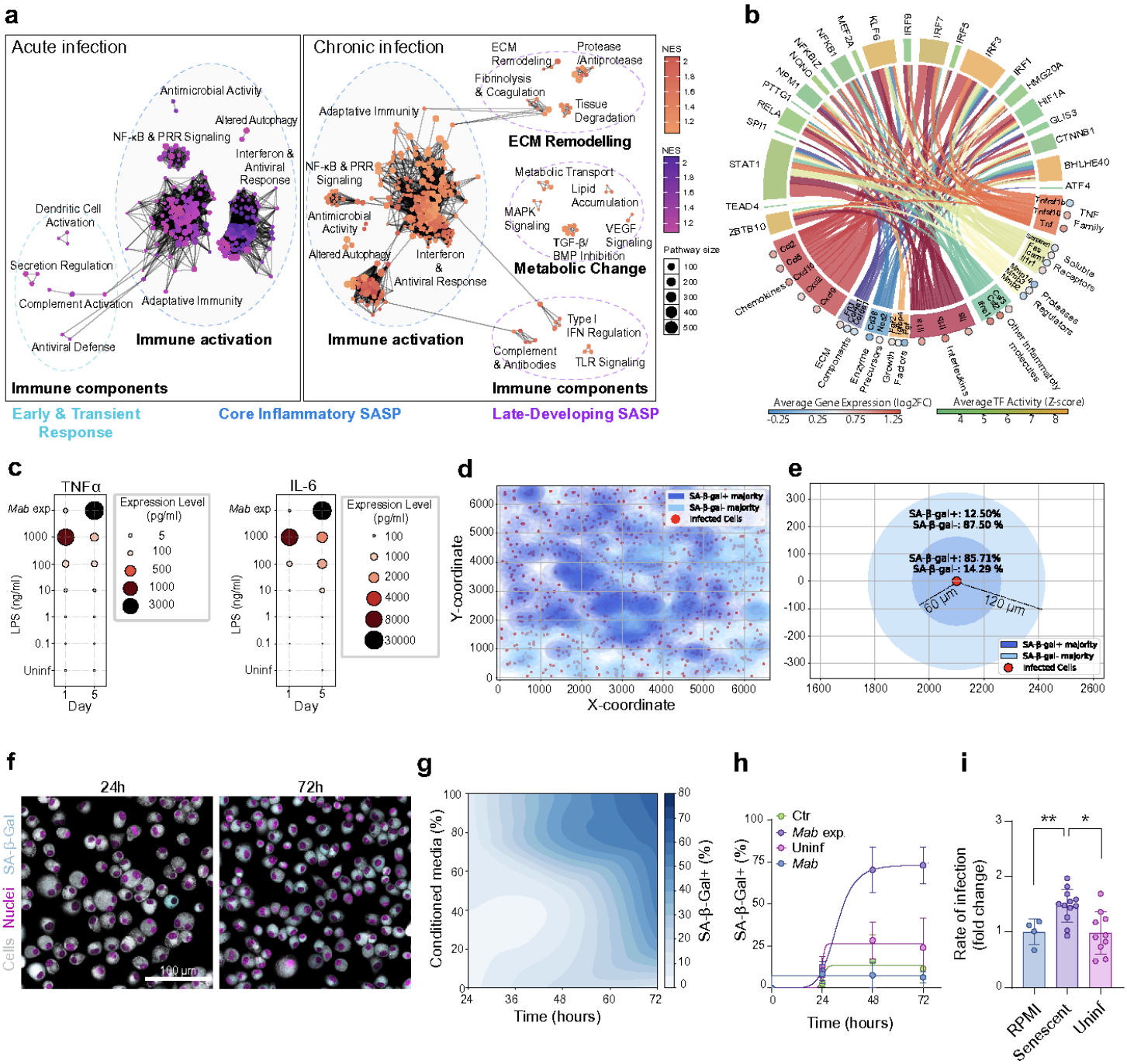


Figure 4

a, Integrated pathway enrichment network analysis depicting relationships between enriched biological processes and pathways in *Mab* exposed senescent cells compared to uninfected controls after 1 day (acute infection, left) or 5 days (chronic infection, right) of pathogen exposure. Dotted circles delineate functional modules: cyan circles indicate “early & transient responses” present only during acute infection; blue circles represent “core inflammatory SASP” pathways present at both timepoints; violet circles indicate “late-developing SASP” modules emerging only during chronic infection. Node size represents pathway size; node colour indicates normalised enrichment score (NES); grey connecting

lines depict functional relationships between pathways. b, Circular chord diagram showing the upstream transcription factor (TF) regulatory networks, predicted from IPA analysis, for chronically exposed senescent cells (5 days) vs time-matched uninfected controls. *Top-half ring* segments represent individual transcription factors, colour-coded by average activity (Z-score). *Lower-half* ring segments represent target genes of these TFs, divided into macro-classes of different colours. Connecting ribbons link transcription factors to their target genes. Coloured-coded dots represent the average expression of target genes (log2FC). c, ELISA quantification of key SASP factors (TNFα on the left and IL-6 on the right) in MPI cells exposed for 1 or 5 days to *Mab*, LPS (ranging from 0.1 to 1000 pg/ml), or uninfected controls. Colour intensity indicates concentration level (white, low; red/brown, high; black, exact concentration). d, Spatial distribution of *Mab*$^{+}$ (red dots) and surrounding prevalence of SA-β-Gal^{+} (dark blue) or SA-β-Gal^{-} cells (light blue). **e**, Quantitative analysis showing the percentage of SA-β-Gal^{+} or SA-β-Gal^{-} cells within a range of 60 or 120 µm from a *Mab*$^{+}$ cell. f, Representative confocal microscope images of uninfected MPI cultured for up to 72 hours with 75% (v/v) conditioned media (CM) from chronically *Mab* exposed cells and stained for SA-β-Gal. Cell nucleus (Hoechst, magenta), SA-β-Gal (C12FDG, cyan), cell (Cellmask, grey). Scale bar 100µm. g, Contour plot showing the percentage of SA-β-Gal^{+} cells over time upon incubation with different dilutions of conditioned media isolated from *Mab* exposed cells. h, Quantification of SA-β-gal^{+} cell accumulation in response to treatment with different CM. Ctr (classical RPMI media), *Mab* exp. (CM from senescent *Mab* exposed cells), Uninf (CM from uninfected cells cultured for 5 days), *Mab* (RPMI spiked with *Mab* for 24 hours and then filtered). Data represent mean ± s.d (n = 3 independent experiments). i, Quantification of infection rate as fold change. Bar graph comparing rate of infection (fold change) across cells incubated with three different media: classical RPMI media, CM from *Mab* exposed senescent cells, and CM from uninfected cells. Data represent mean ± s.e.m. **p < 0.01, *p < 0.05, one-way ANOVA with Tukey's post hoc test. CM is conditioned media.

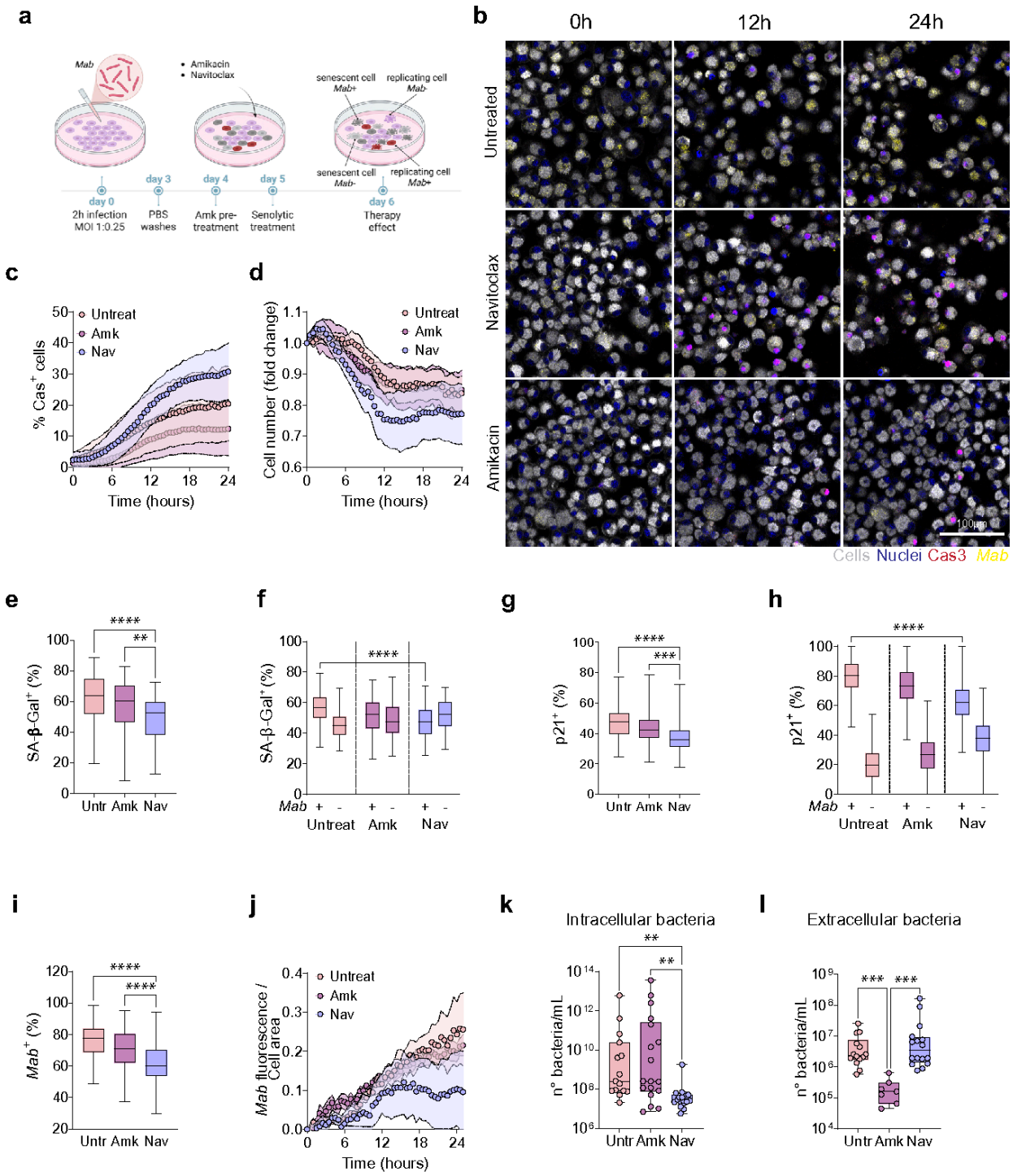


Figure 5

a, Schematic diagram of the chronic *Mab* infection protocol and senolytic treatment. Infection begins on day 0 with a low multiplicity of infection (MOI) for 2 hours, followed by PBS washes. At day 4, Amikacin is added to eliminate extracellular bacteria. At day 5, senolytic treatments are administered for 24 hours. Biorender generated by Doriana Oliveri. **b,** Representative immunofluorescence images of *Mab* exposed cells, at different time points after senolytic or Amikacin treatment. Cell nucleus (Hoechst, blue), cell

(Cellmask, grey), Cas3 (488 Green Caspase 3 dye, red) and *Mab* (tdTom, yellow). Scale bar 100µm. **c**, Percentage of Cas3 positive cells overtime following Amikacin or Navitoclax treatment. **d**, Number of cells overtime following Amikacin or navitoclax treatment, represented as fold change over untreated control at time 0. **e-i**, Percentage of SA-β-Gal positive (**e,f**), p21 positive (**g,h**) or *Mab* positive (**i**) cells after treatments with Amikacin or Navitoclax. Comparison between the whole infected population (**e,g,i**) or between Mab^{+} and Mab^{-} cells (**f,h**). Non parametric one-way ANOVA (Kruskal-Wallis test) analysis (** p<0.01, *** p<0.001, **** p<0.0001). At least 1000 cells per condition. **j**, Quantification of *Mab* fluorescence (TdTom) to cell area (Cellmask) ratio over time after treatment with Amikacin or Navitoclax. **k-l**, Bacterial concentration from CFU assay expressed as number of bacteria per ml, in cell lysate (**k**) representing intracellular bacteria or cell supernatant (**l**) representing extracellular bacteria. Non parametric one-way ANOVA (Kruskal-Wallis test) analysis (** p<0.01, *** p<0.001). At least seven biological replicates.

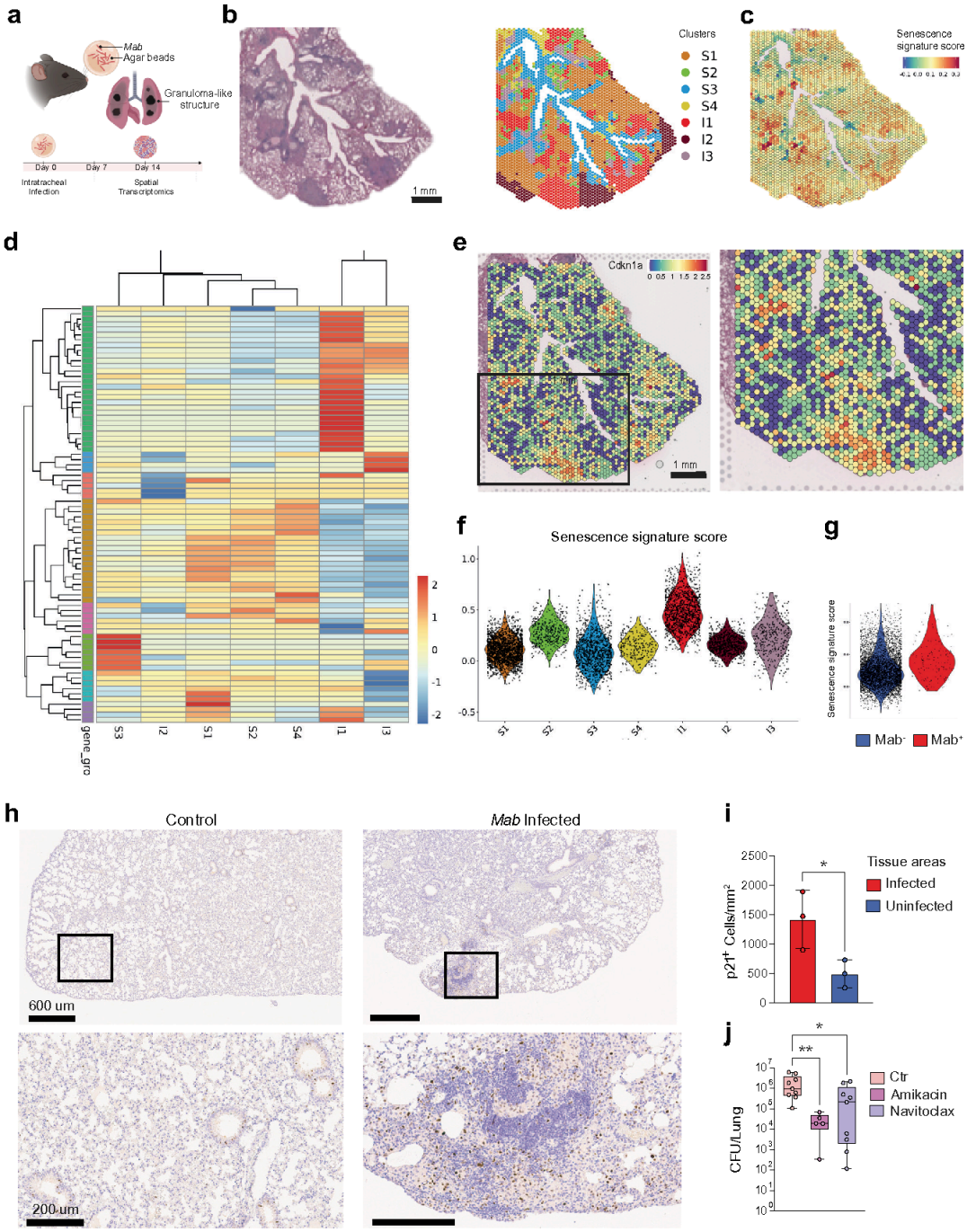


Figure 6

a, Schematic representation of a mouse model of infection (Created in Biorender generated by Edoardo Scarpa). **b**, (left) H&E staining of chronically infected lungs used for spatial transcriptomic (Scale bar, 1 mm); (right) Spatial dimensionality plot in a slice from a mouse with a chronic infection, colour-coded by transcriptional clusters. The spots are arranged according to their spatial coordinates in the tissue sections (Scale bar, 1 mm). **c**, Spatial plot showing the values of the senescence signature score in a

slice from a mouse with a chronic infection (Scale bar, 1 mm). **d**, Heatmap of SenMayo gene set[28] expression across different cell clusters. Genes are hierarchically clustered by expression pattern. Colour intensity indicates z-scored normalised expression values (red, upregulated; blue, downregulated). **e**, Spatial plot showing the expression levels of Cdkn1a in a slice from a mouse with a chronic infection (Scale bar, 1 mm). **f**, Violin plot showing the senescence signature score in the various clusters. **g**, Violin plot showing the senescence signature score in *Mab*$^{+}$ and *Mab*$^{-}$ spots. **h**, Immunohistochemistry staining for p21 in control and *Mab* infected lungs (Scale bar, 600 mm and 200 mm). **i**, Quantification of p21^{+} cells/mm^{2} of tissue in infected or uninfected areas of the same tissue (t-test, *p<0.05). **j**, Quantification of lung CFUs in untreated, Amikacin or navitoclax treated mice. (**p < 0.01, *p < 0.05, one-way ANOVA with Kruskal-Wallis post hoc test).

Supplementary Files

This is a list of supplementary files associated with this preprint. Click to download.

- extendedFig1.pdf
- extendedFig2.pdf
- extendedFig3.pdf
- extendedFig4.pdf
- extendedFig5.pdf
- extendedFig6.pdf